Proceedings of ASME Turbo Expo 2011
GT2011
June 6-10, 2011, Vancouver, British Columbia, Canada

GT2011-46013

Flow and Heat Transfer in the Tip-Turn Region of a U-Duct under Rotating and Non-Rotating Conditions

S.-Y. Hu[1], X. Chi[1], T.I-P. Shih[1,2], K.M. Bryden[2], M.K. Chyu[3], R. Ames[4], and R.A. Dennis[4]

[1]School of Aeronautics and Astronautics, Purdue University, West Lafayette, IN 47905
[2]Ames Laboratory, U.S. Department of Energy, Ames, IA 50011
[3]Department of Mechanical Engineering and Material Science, University of Pittsburgh, Pittsburgh, PA 15261
[4]National Energy Technology Laboratory, U.S. Department of Energy, Morgantown, WV 26507

ABSTRACT

CFD simulations were performed to study the flow and heat transfer in a U-duct, relevant to internal cooling of the first-stage turbine component in electric-power-generation, gas-turbine engines. Parameters studied include (1) two aspect ratios of the duct cross section, i.e. H/W=1 and H/W=0.25; (2) smooth duct and duct lined with pin fins of height H arranged in a staggered fashion; and (3) two rotational speeds: 0 rpm and 3,600 rpm. In all cases, the wall temperature is 1173 K; the coolant temperature at the U-duct inlet is 623 K; and the back pressure at the exit of the U-duct is 25.17 atm. The Reynolds numbers studied are 150,000 for the duct with the 4-to-1 aspect ratio, and 150,000 and 375,000 for the duct with the 1-to-1 aspect ratio. When there is rotation at 3,600 rpm, the rotational numbers corresponding to these Reynolds numbers and duct aspect ratios are 0.592, 1.64, and 4.11, respectively. Result is presented to show the nature of the flow, the temperature distribution, and the surface heat transfer with focus on the flow and heat transfer in the tip-turn region as a function of the parameters investigated. This computational study is based on 3-D steady RANS. The ensemble-averaged continuity, compressible Navier-Stokes, and energy equations were closed by the thermally perfect equation of state with temperature-dependent gas properties and the two-equation realizeable k-ε turbulence model with and without wall functions.

NOMENCLATURE

D	diameter of the pin fins
D_h	duct hydraulic diameter
h	heat transfer coefficient, $q''/(T_b - T_w)$
H	height of the U-duct in Z-direction
k	thermal conductivity
L	length of the U-duct
L_x	distance between pin fins in X-direction
L_y	distance between pin fins in Y-direction
Nu	Nusselt number, hD_h/k
p_i	spacing between pin fins and pin fin and inner/outer walls
P_b	static pressure at the U-duct exit (if an extension is added, then it is the distance R from the axis of rotation or X = W-L)
Pr	Prandtl number
q”	heat flux
Re	Reynolds number, $\rho U D_h/\mu$
Ro	rotation number, $\Omega D_h/U_{inlet}$
T	temperature
T_b	bulk temperature
T_{inlet}	coolant temperature at the U-duct inlet
T_w	wall temperature
U_{inlet}	mean velocity in duct at the inlet
U_τ	friction velocity, $(\tau/\rho)^{0.5}$
W	width of the duct cross section
X	coordinate along duct span wise direction (see Fig. 1)
y	normal distance from wall
y^+	$\rho U_\tau y/\mu$
Y	coordinate along duct legs direction (see Fig. 1)
Z	coordinate defined in Fig. 1

Greek Symbols

ρ	density
Δρ/ρ	density ratio, $(T_w - T_{inlet})/T_w$
μ	dynamic viscosity
Ω	rotational speed
τ	wall shear stress

INTRODUCTION

Gas turbines for electric-power generation and aircraft propulsion have undergone tremendous advances during the past few decades. Though great progress has been made, there is still opportunity to improve efficiency and service life. For gas turbines, high efficiency demands high temperatures at the turbine inlet, and long service life demands effective cooling with minimum cooling flow to ensure material temperatures do not exceed the maximum allowable for strength and durability [1-10]. In the past, the goal has been to increase efficiency by increasing the turbine inlet temperature without increasing the cooling flow. Today, the goal is to maintain the high turbine inlet temperatures but substantially reduce the cooling flow by as much as 50%.

With this new goal, there are two critical needs. The first is the need for innovative and revolutionary cooling strategies that could accomplish the goal. The second is the need for markedly improved understanding of the flow and heat transfer that ensures effective and nearly uniform cooling with minimal cooling flow. One area in internal cooling, where improved understanding is very much needed, is the flow and heat transfer in the tip-turn region inside internal cooling passages with high aspect-ratio-cross sections.

Reviews of studies on internal cooling have been reported by Refs. [5-10]. Shih & Sultanian [8] summarized computational studies of the flow and heat transfer in straight and U-ducts up to 2000. Besserman & Tanrikut [11], Wang & Chyu [12], and Rigby *et al.* [13] studied non-rotating smooth ducts with 180^o bends. Iacovides *et al.* [14,15], Medwell *et al.* [16], Tekriwal [17], Dutta *et al.* [18], Tolpaldi [19], Stephens *et al.* [20], Hwang *et al.* [21], Stephens & Shih [22], and Chen *et al.* [23] studied rotating and non-rotating smooth ducts. Prakash & Zerkle [24, 25], Abuaf & Kercher [26], Stephens *et al.* [27], Rigby *et al.* [28], Rigby [29], and Bohn *et al.* [30] studied ducts with normal ribs in non-rotating ducts. Inclined ribs in rotating and non-rotating ducts were studied by Stephens *et al.* [31], Bonhoff *et al.* [32, 33], Stephens & Shih [34], Shih *et al.* [36, 37], Jang, et al. [37], Lin, et al. [35, 39], Shih, et al. [40], Zehnder, et al. [41], and Schüler, et al. [42].

Of the 3-D studies, most used wall functions to bridge the high-Reynolds number region of the turbulent flow and the wall. The exceptions are Stephens *et al.* [20, 27, 31], Stephens & Shih [22, 34], Shih *et al.* [36, 37, 40], Rigby *et al.* [28, 29], Chen *et al.* [23], Jang, et al. [38], Lin, et al. [35, 39], Zehnder, et al. [41], and Schüler, et al. [42] who used low Reynolds number turbulence models in which the integration is all the way to the wall. Shih, Stephens, Lin, and co-workers [20, 22, 27, 31, 34-37, 39, 40], Zehnder, et al. [41], and Schüler [42] used the low-Reynolds number shear-stress transport (SST) model [43, 44]. Rigby and co-workers used the k-ω model [43, 45]. Chen and co-workers [23, 38] used a low Reynolds number differential Reynolds stress model (DSM). On studies of rotating ducts, most invoked the incompressible flow assumption with the Boussinesque approximation for the buoyancy effect because the rotational number, density ratio, and Mach numbers were low. The exceptions are the studies by Shih, Stephens, Lin, and co-workers [20, 22, 34-37, 39, 40] and Rigby, et al. [29] who used the compressible Navier-Stokes equations so that centrifugal buoyancy can be accounted for. On geometry, most computational studies have focused on ducts of square cross section. Zehnder, et al. [41] and Schüler [42] performed experimental and computational studies of a U-duct with engine-similar trapezoidal cross sections for both smooth walls and walls lined with inclined ribs.

A number of investigators have used experimental methods to study the heat transfer in ducts of different cross sections (see Han, et al. [5] for a review). Taslim [46, 47] studied rib-roughened straight ducts with cross sections H/W ranging from 0.25 to 3.5, where W is the width of the duct and is the surface of the duct on which ribs are mounted, and H is the height of the duct and is the parameter being varied to achieve different duct aspect ratios. Taslim [46, 47] showed that the Nusselt number is proportional to the Reynolds number raised to the 0.6 power for a variety of ribs mounted on two opposite walls of the duct for fully developed flow in a straight duct. For a given rib configuration, the higher the blockage from the rib height, the higher is the Nusselt number. Taslim [46] also showed that for a given rib configuration, the friction factor is independent of the Reynolds number. However, the smaller the aspect ratio, the higher is the friction factor.

Pin fins in high-aspect ratio ducts have been studied for enhancing cooling in the trailing-edge region [48-56]. Most studies focused on an array of pin fins in which the pin fins have a circular cross section (see review by Han, et al. [5]). For an array of pin fins arranged in a staggered fashion, Chyu, et al. [54] showed that the Nusselt number is also proportional to the Reynolds number raised to about 0.6 power. However, the heat transfer through the surface of the pin fins is appreciably higher than the heat transfer through the walls of the duct, which is a function of H/D, where H is the height of the pin fin and D is the diameter of the pin fin. The heat transfer through the pin fins and the duct walls is enhanced through the wakes behind each pin fin, the interactions among the wakes, and the horseshoe vortices that wrap around the two ends of each pin fin where it touches the duct walls. For an array arranged in a non-staggered fashion, Chyu, et al. [54] showed a stronger dependence on the Reynolds number (instead of a 0.6 power, it ranges from 0.658 to 0.759).

So far, experimental and computational studies have not been reported on the flow and heat transfer in high-aspect ratio U-ducts mounted with pin fins under rotating and non-rotating conditions. The region around the tip-turn is of particular interest, because of complicating factors that can result. For example, a staggered array of pin fins may appear as non-staggered in the tip turn region because the main-flow direction is changed by the turning portion of the U-duct. Also, complex secondary flows are set up by the turning and by the rotation. The objective of this study is to perform a CFD study to understand the flow and heat transfer in a high-aspect ratio U-duct lined with a staggered array of pin fins under rotating and non-rotating conditions.

The remainder of this paper is organized as follows. First, the U-duct problem studied, the problem formulation, and the numerical method of solution are described. Next, results from a grid sensitivity study are given followed by results for the flow and heat transfer in the U-duct.

DESCRIPTION OF THE PROBLEM

Figure 1 shows a schematic of the configurations studied. There are two types of U-ducts, one with smooth walls and one with a staggered array of pin fins that extend from wall to wall in the Z direction. For both types of ducts, two aspect ratios of the duct-cross section were studied, H/W = 1 and 0.25, where W = 5.715 cm (2.25 inches). For the duct with pin fins, each pin fin has diameter D = 0.635 cm (0.25 inches) and are separated by $p_1 = p_2 = 1.5875$ cm (0.625 inches) in the Y and X directions, respectively, where p_1 and p_2 are pin center to pin center distances. The distance from the pin center to the inner and outer wall is p_3 = 1.27 cm (0.5 inches). For all of the U ducts studied, the total length of the duct, which includes the up/down leg and the turn region is L = 38.1 cm (15 inches), and the distance that separate the up and the down legs of the U-duct is t = 0.635 cm (0.25 inches). The inlet of the U-duct is located at R = 38.1 cm (15 inches) from the axis of rotation.

For the aforementioned two U-ducts, the wall temperature was maintained at T_w = 1173 K; the coolant temperature at the duct inlet was uniform at T_{inlet} = 623 K; the pressure at the duct exit was kept constant at P_b = 370 psi (the duct exit is defined as the distance R from the axis of rotation or Y = W–L); and the turbulence intensity at the duct inlet was set at 5%. For the smooth and the pin-finned U-duct with H/W = 0.25, the Reynolds numbers (Re) based on the hydraulic diameter (D_h = 0.9 inches), T_{inlet}, and P_b was 150,000, which was achieved by setting the speed of the coolant flow at the duct inlet to be uniform at U_{inlet} = 14.56 m/s. For smooth and pin-finned U-duct with H/W =1 (D_h = 2.5), two Reynolds numbers were studied, 150,000 and 375,000. To achieve Re = 150,00 and 375,000, the speed of coolant flow at the duct inlet was set to be uniform at U_{inlet} = 5.824 m/s and U_{inlet} = 14.56 m/s, respectively. The Re = 375,000 was studied for the case with H/W = 1 because the U_{inlet} is the same as the U_{inlet} for the cases with H/W = 0.25. Note that when the flow is not "fully" developed, the meaningful Reynolds number is not based on the duct hydraulic diameter, but rather the distance from the leading edge of the boundary later. Two rotational speeds, Ω, of the U-ducts were studied, stationary and 3,600 rpm. When the rotational speed is 3,600 revolutions per minute, the corresponding rotational number is 0.592 for H/W = 0.25 and Re = 150,000, 1.64 for H/W = 1 and Re = 150,000, and 4.11 for H/W = 1 and Re = 375,000.

All cases studied are summarized in Table1. The geometric and operating parameters were selected to approximate engine operating condition.

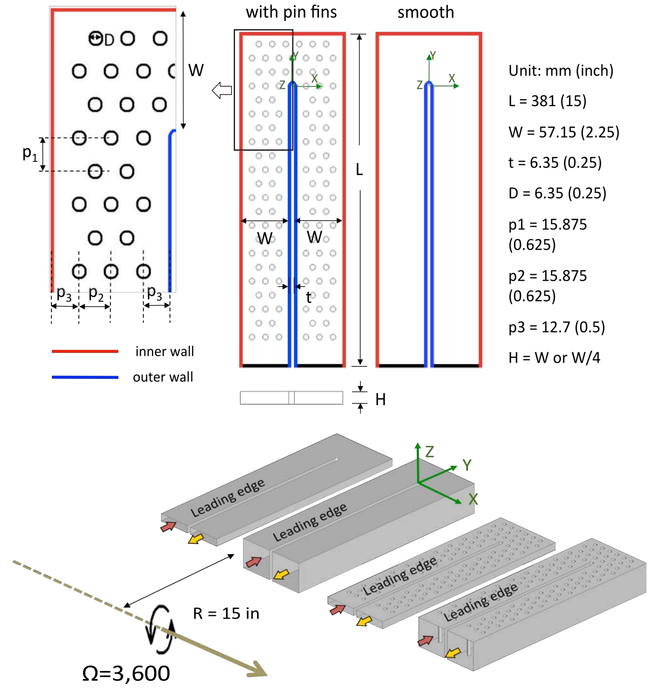

Fig. 1. Schematic of the U-ducts studied.

Table 1. Summary of Cases Studied*

Case #	Ω (rpm)	smooth or w/ pin fins	H/W	U_{inlet} (m/s)	D_h (Inch)	Re	Ro
1	0	smooth	1	5.824	2.5	150,000	0
2	0	smooth	1	14.560	2.5	375,000	0
3	0	smooth	0.25	14.560	0.9	150,000	0
4	0	pin fins	1	5.824	2.5	150,000	0
5	0	pin fins	1	14.560	2.5	375,000	0
6	0	pin fins	0.25	14.560	0.9	150,000	0
7	3,600	smooth	1	5.824	2.5	150,000	4.11
8	3,600	smooth	1	14.560	2.5	375,000	1.64
9	3,600	smooth	0.25	14.560	0.9	150,000	0.592
10	3,600	pin fins	1	5.824	2.5	150,000	4.11
11	3,600	Pin fins	1	14.560	2.5	375,000	1.64
12	3,600	pin fins	0.25	14.560	0.9	150,000	0.592

* T_w = 1173 K, T_{inlet} = 623 K, P_b = 370 psi, turbulent intensity at inlet = 5%, Δρ/ρ = 46.8%.

FORMULATION OF PROBLEM, NUMERICAL METHOD OF SOLUTION, AND CODE

The problems described in the previous section involve a gas whose density can change significantly from the large differences in the wall and coolant temperature and from rotation even though the relative Mach number of the flow is quite low. The governing equations used are the ensemble-averaged continuity, full compressible Navier-Stokes, and energy equations for a thermally perfect gas with temperature dependent thermal conductivity, viscosity, and specific heats for air. The effects of turbulence were modeled by the two-equation realizable k-ε model [57]. In the near-wall region, two treatments were investigated: enhanced wall functions [58] and the one-equation two-layer model of Chen and Patel [59]. The Chen and Patel model divides the turbulent flow field into two regions. One region, referred to as the wall region, extends from the wall to the edge of the fully turbulent region. The other region, referred to as the core region, contains the rest of the turbulent flow field which is fully turbulent everywhere. In the wall region, the one-equation model of Wolfshtein [60] is used, and in the core region, the realizable k-ε model is used.

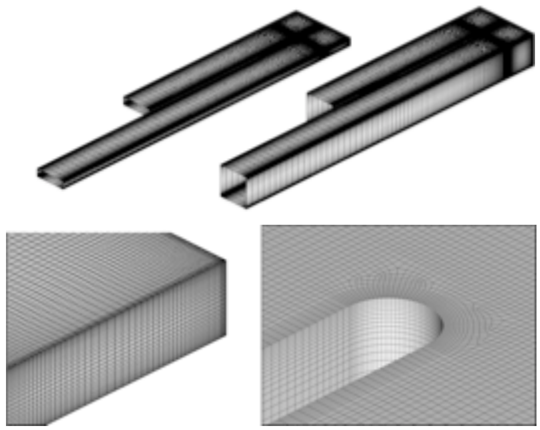

Fig. 2. Grid for the smooth U-duct.

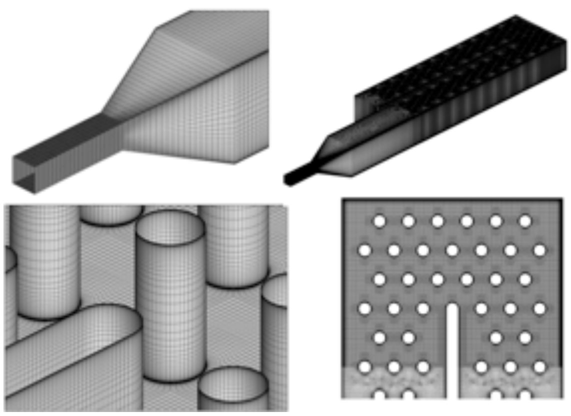

Fig. 3. Grid for the U-duct with pin fins.

Figures 2 and 3 show an example of the grids used to obtain solutions. Note that for the smooth ducts, an extended straight section was appended to the exit of the U-duct. This was added to ensure that there is no flow reversal at the outflow boundary. For the U-ducts with pin fins, the extended section also had a contraction to accelerate the flow. With the contraction, no flow reversal at the outflow boundary can be achieved by using a shorter appended section. For both the smooth and the pin-finned duct, three sets of grids were used, a baseline grid for use with the enhanced wall function, where y^+ of the first cell away from walls varied from 10 to 40; a fine grid for use with the low-Reynolds number model of Chen and Patel in the near-wall region, where y^+ of the first cell away from walls is less than unity; and a further refined grid to test the adequacy of the fine grid in resolving the flow in the near-wall region. The third refined grid was derived from the fine grid by using H-refinement next to walls. For the smooth duct, the number of cells in the baseline, fine, and refined grids are 1.8 million, 4.1 million, and 6.2 million, respectively when H/W = 1, and 1.1 million, 4.1 million, and 6.2 million, respectively when H/W = 0.25. For the pin-finned duct, the fine and the refined grids only had grids added in the turn region, but the rest of the duct still had the same distribution as the baseline grid. For the pin-finned duct, the baseline grid had 5.7 million cells when H/W = 1 and 4.1 million cells when H/W = 0.25. The fine grid had 7.4 million cells when H/W = 0.25, and the refined grid had 9.6 million cells when H/W = 0.25.

Solutions to the governing equations were obtained by using Version 12.0 of the Fluent UNS code [60]. Only steady-state solutions were sought, and the SIMPLE algorithm was used to generate solutions. All equations were integrated over each cell of the grid system. The fluxes for density, momentum, and energy at the cell faces are interpolated by using the second-order upwind scheme. Pressure was also computed by using second-order accuracy. For all computations, iterations were continued until all residuals for all equations plateau to ensure convergence to steady-state has been reached. When the flow is turbulent, the normalized residual is always less than 10^{-5} for the three components of the velocity, less than 10^{-7} for the energy, less than 10^{-5} for turbulent kinetic energy, less than 10^{-4} for dissipation rate of turbulent kinetic energy, and less than 10^{-3} for the continuity equation.

RESULTS

Grid-Sensitivity Study and Effects of Wall Function

Figure 4 shows the error in the computed heat flux along the up-leg wall at X = -(W+t)/2 and Z = H/2 and along the down-leg wall at X = (W+t)/2 and Z= H/2. From Fig. 4, it can be seen the "fine" grid predicted lower heat flux than the "baseline" grid by 10 to 20%. Thus, wall functions over predict surface heat transfer. From Fig. 4, it can also be seen that the "fine" and the "refined" grids give nearly identical results (< 1% difference), indicating that the fine grid gives grid-independent solutions.

Figure 5 shows the computed total pressure and projected streamlines in the middle plane (Z = 0) by using "enhanced" wall functions on the baseline grid (y^+ of first cells next to walls between 10 and 20) and by using the low-Reynolds number model of Chen and Patel on the fine grid (y^+ of first cells next to walls less than unity). From this figure, it can be seen that the solutions computed on the baseline grid and on the fine grid provide similar flow features. Both could capture the main features of the flow such as the wakes behind each pin fin and the separated region around the 180^{o} bend. The finer grid does, however, capture more details of those features because of the higher resolution.

All results given in the Results section are generated by using the fine grid.

Nature of the Flow

Figures 6 to 12 show the nature of the flow. The key flow features in the U-duct are the secondary flow induced by the Coriolis force (Fig. 6), the Dean-type secondary flow induced by the 180^0 bend (Fig. 7), the flow separation about the bend in the down-leg part of the U-duct (Fig. 8) due to the adverse pressure gradient induced by flow turning, the asymmetry in the flow and temperature distribution from the leading face to the trailing face of the

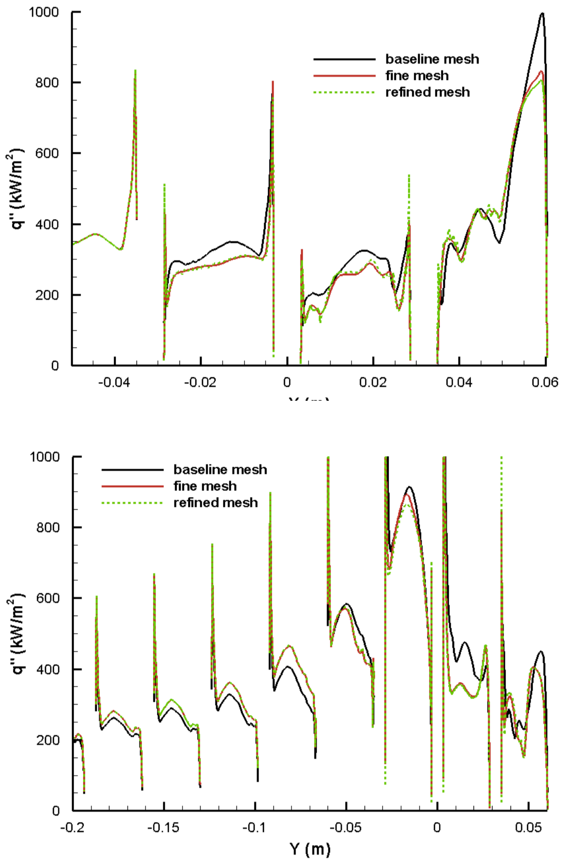

Fig. 4. Grid-sensitivity study. Top: q” along up-leg at X=-(W+t)/2 and Z = H/2. Bottom: q” along down-leg at X = (W+t)/2 and Z = H/2.

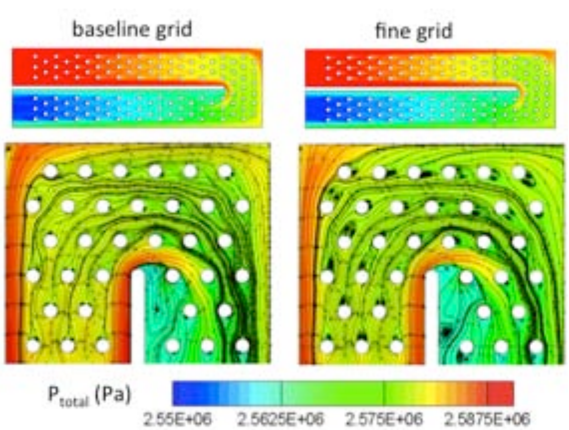

Fig. 5. Total pressure and projected streamlines in the middle plane about the turn region ($\Omega = 0$) computed on the baseline and fine grids.

U-duct due to rotation (Fig. 9), flow separation on the leading face in the up-leg part due to centrifugal buoyancy (Fig. 10), and pin-fin induced wakes and horseshoe vortices (Figs. 11 and 12). Note that counter-rotating vortices at the four corners of the duct-cross section created by the anisotropy of the turbulence were not observed. This is because the turbulence model used assumed isotropy of the turbulence. Ref. 35 showed that these secondary flows are weak when compared to other secondary flow structures due to rotation and ribs.

The large separated region on the leading face induced by centrifugal buoyancy was found to dominate the flow in the up-leg part of the U-duct. Figure 10 shows the size of the separated region on the leading face along the Y and Z directions to be smaller when H/W is smaller. The separated region is about 0.9 L x 0.8 H in size when H/W = 1 and about 0.8 L x 0.3 H in size when H/W = 0.25. With pin fins, the size of the separated region is reduced. This is because pin fins increase mixing, which makes the flow next to the wall boundary layer fuller and because the pin fins increase resistance to reverse flow. Nevertheless, the separated region was still quite appreciable in size when H/W = 1.

At section S1 in Fig. 6, the pair of counter-rotating secondary flow induced by the Coriolis force can be seen in the smooth U-duct when H/W = 0.25, but not when H/W = 1 because of the large separated region induced by centrifugal buoyancy. When there are pin fins, the horseshoe vortex that wraps around each pin fin dominates the structure of the secondary flow in their vincinity, though Corilois force still play a role in creating the asymmetry from the leading and trailing faces. At section S2, the curvature in the flow induced by the upstream turn region amplified the recirculating flow that is consistent with the flow directions of the Dean-type secondary flows. Even when there are pin fins, the effects of the dean-type secondary flow can be seen between the outer wall and the pin fin and between the pin fins.

At section 3 in Fig. 7, the symmetric counter-rotating Dean-type secondary flow can be seen in the smooth duct when there is no rotation. The effect of reducing H/W from 1 to 0.25 is to shift the centers of the two recirculating flows towards the inner and the two . The effect of the increasing the Reynolds number is the same. One reason is that when the H/W is decreased while holding the Reynolds number constant or when the Reynolds number is increased while holding H/W constant, the core or main-stream flow speed is increased so that the jet-like flow in the turn region pushes the secondary flows effects towards the side and inner walls, where the flow speed is lower. When there are pin fins, the structure of the Dean-type secondary flow can still be seen between the pin fin and the inner and the outer wall, albeit made more complicated by the wakes behind the pin fins and by the horseshoe vortices that wrap around pin fins. When there is rotation, the Dean-type secondary flow reduces to one recirculating flow structure. This structure persists even when there are pin fins.

Figure 8 shows the flow structure in the middle plane (Z=0) for rotating and non-rotating smooth U-duct. From this figure, it can be seen that there are three separated regions in the turn region: two at the corners on the U-duct and one around the bend. The size of these separated regions is larger when H/W is smaller or when the Reynolds number is larger. Rotation reduces the size of the separated region about the bend. Figure 9 shows how rotation effects the flow in the X-Y planes along the Z direction for smooth U-duct. Figures 4 and 12 show that the pin fins behaved like guide vanes. The pin fins next to the outer wall create a passage for the coolant that hugs the outer wall, and this eliminated the two separation bubbles in the two corners of the U-duct in the turn region (Fig. 4). Similarly, the pin fins next to the inner wall formed a passage for the coolant that hugs the inner wall, which greatly reduced the size of the separation bubble around the bend, bounding it between three rows of staggered pin fins (Fig. 4). In the turn region, the "staggered array of pin fins" behaved like a "nonstaggered array of pin fins" that do not obstruct but guide the turning of the flow (Figs. 4 and 12).

Figure 11 shows that the wake structure behind the pin fins is larger at the base of the pin fins where they are mounted (Z = -H/2, H/2) than at the mid plane (Z = 0). This is because at the base of the pin fin, there is a horseshoe vertical structure in addition to the flow separation about a circular cylinder.

Nature of the Heat Transfer

For this problem, the flow and heat transfer are intimately connected. For example, centrifugal buoyancy occurred next to the leading face because Coriolis induced secondary flow caused the coolant next to the leading face to be hotter. Nevertheless, in this section, the heat transfer on the U-duct walls is explained in terms of the fluid mechanics.

Figures 13 to 16 show the heat flux on the side and outer walls of the U-duct. From these figures, the following observations can be made. For a smooth U-duct without rotation, heat flux decreases along the U duct until it reaches the turn region because of the developing boundary layer. In the turn region, heat flux is high on the outer wall and the side walls(leading and trailing walls) because the Dean-type secondary flow transported the coolant in the core of the duct with lower temperature to the outer wall and then the side walls. Also, the core flow impinges on the outer wall as it turns around the bend. Around the bend, heat flux is high on the outer wall and the side wall because the separated region cause the flow around the bend to speed up and impinge on the outer wall. The heat flux then decreases along the down-leg part of the U-duct.

It is important to note that the heat flux in the up-leg part of the U-duct for the following two cases are almost identical: H/W = 1 & Re = 375,000 (Case 2) and H/W = 0.25 & Re = 150,000 (Case 3). The reason for the similarity is that these two cases have the same inlet speed (14.56 m/s) and boundary layer in the U-duct starts at the duct inlet. When the boundary layers from four walls of the duct have not yet merged, the meaningful Reynolds number is not based on hydraulic diameter but distance from the leading edge of the boundary layer. Thus, Cases 1 and 3 have essentially the same Reynolds number in the up-leg part of the U-duct. This similarity can also be seen in Fig. 10.

When there are pin fins, heat transfer is highest on the leading edge of each pin fin where the flow impinges on it. On the side walls where pin fins are mounted, heat flux is highest in the region about the horseshoe vortex that wraps around each pin fin and lowest in the wakes just behind each pin fin. On the side walls, Fig. 14 shows the heat flux to be also high in the region between the pin fins and the outer wall and in the region between the pin fins and the inner wall, where pin fins served as guide vanes and turbulence generators.

When there is rotation, Figs. 15 and 16 show that heat flux on the leading face is considerably lower than that on the trailing face in the up-leg because of centrifugal buoyancy induced flow separation on the leading face. In the turn region, heat flux is high on the leading face because of the reattachment of the separated region. In the down-leg part of the duct, the heat flux on the leading face is higher than that on the trailing face.

Effects of H/W, Pin Fins, and Rotation on Total Heat Transfer and Total Pressure Drop

Figure 17 shows the total heat transfer from the U-duct for all cases studied with Re = 150,000. From this figure, it can be seen that heat transfer is highest when H/W = 1 with pin fins and rotation, followed by H/W = 1 with pin fins but no rotation, H/W = 1 without pin fins and rotation, H/W = 0.25 with pin fins and rotation, H/W = 0.25 with pin fins and no rotation, H/W = 0.5 with rotation and no pin fins, H/W = 1 without rotation and pin fins, and H/W=0.25 without rotation and pin fins. Basically, two things dominated: (1) surface area whether the increased area is from H/W (recall that W was fixed, but H changed) or pin fins and (2) whether there is rotation or not. When there are pin fins in the U-duct, the heat transfer from the pin fins is appreciable and higher than the heat transfer from the side, outer and inner walls combined.

Figures 18 and 19 show the net heat transferred (Q = q" x area) and the average heat flux (q") in the up-leg part of the U-duct. From these figures, it can be seen that though pin fins transfer a significant portion of the heat, its averaged q" is about twice that from the side walls when there is no rotation and comparable to that on the trailing wall when there is rotation. Also, when there is rotation, Q and averaged q" from the trailing face is always higher than Q and averaged q" from the leading face. However, that difference is higher when H/W = 1 than for H/W = 0.25. This is because with H/W = 0.25, the separation bubble from centrifugal buoyancy was smaller.

Figures 20 and 21 show the net heat transferred (Q) and the average heat flux (q") in the turn region of the U-duct. From these figures, it can be seen that Q and q" are increased by rotation and by having pin fins. The increase is greater for H/W = 1 and less for H/W = 0.25. In the turn region, the q" is almost twice that from the side walls when there is no rotation and comparable to that on the trailing wall when there is rotation.

Figures 22 and 23 show the net heat transferred (Q) and the average heat flux (q") in the down-leg part of the U-duct. From these figures, it can be seen that Q and q" are increased by having pin fins. However, rotation decreased Q and q". In the down-leg part, q" is almost twice that from the side walls with or without rotation.

Figures 24 to 26 show the total pressure drop across the U-duct as well as the total pressure drop across the up-leg, the turn region, and down-leg parts of the U-duct. When there is no rotation, total pressure loss increases with increase in Reynolds number, with decrease in H/W from 1 to 0.25, and with pin fins added. When there is rotation, total pressure loss increases with increase in Reynolds number and with pin fins added. However, it decreases with decrease in H/W from 1 to 0.25. The reason for this can be seen in Figs. 9 and 10. For a smooth U-duct with H/W = 0.25, rotation almost completed removed the separation bubble around the bend in the down-leg part, although the centrifugal buoyancy induced separation bubble formed in the up-leg part.

For smooth ducts, the turn region generated most of the pressure loss. However, when pin fins are added, the up-leg and down-leg generate much greater pressure losses.

CONCLUSIONS

This CFD study based on steady RANS with realizeable k-ε model and enhanced wall functions (y^+ of the first cell between 10 and 20) show the following:

- When there is rotation, centrifugal buoyancy induces a large separated region on the leading face of the up-leg. The size of this separation bubble is reduced when H/W is reduced from 1 to 0.25.
- There are three separation bubbles in the turn region: two at the corners on the U-duct and one around the bend. The size of these separated regions is larger when H/W is smaller or when the Reynolds number is larger. Rotation reduces the size of the separated region about the bend.
- The pin fins behaved like guide vanes. The pin fins next to the outer wall eliminated the two separation bubbles in the two corners of the U-duct in the turn region, and the pin fins next to the inner wall greatly reduced the size of the separation bubble around the bend. In the turn region, the "staggered array of pin fins" behaved like a "nonstaggered array of pin fins" that guided the turning of the flow.
- Two things dominated the total surface heat transfer in the U-duct – surface area whether the increased area is from increasing H/W or adding pin fins and whether there is rotation or not. When there are pin fins in the U-duct, the heat transfer from the pin fins is appreciable and higher than the heat transfer from the side, outer and inner walls combined.
- For both smooth and pin-finned U-duct, decreasing H/W from 1 to 0.25 increases average heat flux. When there is rotation, decreasing H/W from 1 to 0.25 reduces the difference in average heat flux from the leading and trailing faces.
- When there is no rotation, loss in total pressure increases with increase in Reynolds number, with decrease in H/W from 1 to 0.25, and with pin fins added.
- When there is rotation, loss in total pressure increases with increase in Reynolds number and with pin fins added. However, it decreases with decrease in H/W.
- For smooth ducts, the turn region generated most of the pressure loss. However, when pin fins are added, the up-leg and down-leg generate much greater pressure losses.

ACKNOWLEDGMENT

This research was supported by the Department of Energy's National Energy Technology Laboratory. The authors are grateful for this support.

REFERENCES

1. Suo, M., "Turbine Cooling," *Aerothermodynamics of Aircraft Engine Components*, Editor: G.C. Oates, AIAA, New York, pp. 275-328, 1985.
2. Metzger, D.E., "Cooling Techniques for Gas Turbine Airfoils," AGARD CP 390, 1985, pp. 1-12.
3. Moffat, R.J., "Turbine Blade Heat Transfer," *Heat Transfer and Fluid Flow in Rotating Machinery*, Editor: W.J. Yang, Hemisphere, Washington, D.C., 1987, pp. 1-24.
4. Goldstein, R.J., "Film Cooling," *Advances in Heat Transfer*, Academic Press, New York, 1971, Vol. 7, pp. 321-379.
5. Han, J.C., Dutta, S., and Ekkad, S.V., *Gas Turbine Heat Transfer and Cooling Technology*, Taylor & Francis, New York, 2000.
6. Goldstein, R., Editor, *Heat Transfer in Gas Turbine Systems*, Annals of the New York Academy of Sciences, Vol. 934, May 2001.
7. Sundén, B. and Faghri, M., Editors, *Heat Transfer in Gas Turbines*, WIT Press, Ashurst, Southhampton, 2001.
8. Shih, T.I-P. and Sultanian, B., "Computations of Internal and Film Cooling," *Heat Transfer in Gas Turbines*, Editors: B. Sundén and M. Faghri, WIT Press, Ashurst, Southhampton, 2001, Chapter 5, pp. 175-225.
9. Shih, T.I-P. and Chyu, M., Guest Editors, *Special Section on Turbine Science and Technology*, AIAA Journal of Propulsion and Power, Vol. 22, No. 2, March-April 2006, pp. 225-396.
10. Lau, S.C., "Enhanced Internal Cooling of Gas Turbine Airfoils," *Heat Transfer in Gas Turbines*, Editors: B. Sundén and M. Faghri, WIT Press, Ashurst, Southhampton, 2001, Chapter 4, pp. 109-173.
11. Besserman, D.L. and Tanrikut, S., "Comparison of

Heat Transfer Measurements with Computations for Turbulent Flow Around a 180 Degree Bend," ASME Paper 91-GT-2, 1991.
12. Wang, T.-S. and Chyu, M.K., "Heat Convection in a 180-Deg Turning Duct with Different Turn Configurations," *AIAA J. of Thermophysics and Heat Transfer*, pp. 595-601, Vol. 8, No. 3, 1994.
13. Rigby, D.L., Ameri, A.A., and Steinthorsson, E., "Internal Passage Heat Transfer Prediction Using Multiblock Grids and a k-ω Turbulence Model," ASME Paper 96-GT-188, June 1996.
14. Iacovides, H. and Launder, B.E., "Parametric and Numerical Study of Fully Developed Flow and Heat Transfer in Rotating Rectangular Ducts," *ASME J. of Turbomachinery*, pp. 331-338, Vol. 113, No. 3, 1991.
15. Iacovides, H., Launder, B.E., and Li, H-Y., "The Computation of Flow Development through Stationary and Rotating U-Ducts of Strong Curvature," *International J. of Heat and Fluid Flow*, pp. 22-33, Vol. 17, 1996.
16. Medwell, J.O., Morris, W.D., Xia, J.Y., and Taylor, C., "An Investigation of Convective Heat Transfer in a Rotating Coolant Channel," *ASME Journal of Turbomachinery*, pp. 354-359, Vol. 113, No. 3, 1991.
17. Tekriwal, P., "Heat Transfer Predictions with Extended k-ε Turbulence Model in Radial Cooling Ducts Rotating in Orthogonal Mode," *ASME J. of Heat Transfer*, pp. 369-380, Vol. 116, No. 2, 1991.
18. Dutta, S., Andrews, M.J., and Han, J.C., "Simulation of Turbulent Heat Transfer in a Rotating Duct," *AIAA J. of Thermophysics and Heat Transfer*, pp. 381-382, Vol. 9, No. 2, 1994.
19. Tolpadi, A.K., "Calculation of Heat Transfer in a Radially Rotating Coolant Passage," *AIAA Paper* 94-0261, 1994.
20. Stephens, M.A., Shih, T.I-P., and Civinskas, K.C., "Computations of Flow and Heat Transfer in a Rotating U-Shaped Square Duct with Smooth Walls," *AIAA Paper* 96-3161, 1996.
21. Hwang, J.-J., Wang, W.-J., and Lai, D.-Y., "Numerical Simulation of Turbulent Heat Transfer and Flow in a Rotating Multiple-Pass Square Channel," *ASME Paper* 97-GT-367, 1997.
22. Stephens, M.A. and Shih, T.I-P., "Flow and Heat Transfer in a Smooth U-Duct with and without Rotation," *AIAA Journal of Propulsion and Power*, pp. 272-279, Vol. 15, No. 2, 1999.
23. Chen, H.C., Jang, Y.J., and Han, J.C., "Computation of Flow and Heat Transfer in Rotating Two-Pass Square Channels by a Reynolds Stress Model," ASME Paper 99-GT-174, June 1999.
24. Prakash, C. and Zerkle, R., "Prediction of Turbulent Flow and Heat Transfer in a Radially Rotating Square Duct," *ASME J. of Turbomachinery*, pp. 835-846, Vol. 114, No. 4, 1992.
25. Prakash, C. and Zerkle, R., "Prediction of Turbulent Flow and Heat Transfer in a Ribbed Rectangular Duct with and without Rotation," *ASME J. of Turbomachinery*, pp. 255-264, Vol. 117, 1995.
26. Abuaf, N. and Kercher, D.M., "Heat Transfer and Turbulence in a Turbulated Blade Cooling Circuit," *ASME J. of Turbomachinery*, pp. 169-177, Vol. 116, 1994.
27. Stephens, M.A., Shih, T.I-P., and Civinskas, K.C., "Computation of Flow and Heat Transfer in a Rectangular Channel with Ribs," *AIAA Paper* 95-0180, January 1995.
28. Rigby, D.L., Steinthorsson, E., and Ameri, A.A., "Numerical Prediction of Heat Transfer in a Channel with Ribs and Bleed," *ASME Paper* 97-GT-431, June 1997.
29. Rigby, D.L., "Prediction of Heat and Mass Transfer in a Rotating Ribbed Coolant Passage with a 180 Degree Turn," *ASME Paper* 98-GT-329, June 1998.
30. Bohn, D.E., Becker, V.J., Kusterer, K.A., Otsuki, Y., Sugimoto, T., and Tanaka, R., "3-D Internal Flow and Conjugate Calculations of a Convective Cooled Turbine Blade with Serpentine-Shaped and Ribbed Channels," *ASME Paper* 99-GT-220, June 1999.
31. Stephens, M.A., Chyu, M.K., Shih, T.I-P., and Civinskas, K.C., "Calculations and Measurements of Heat Transfer in a Square Duct with Inclined Ribs," *AIAA Paper* 96-3163, 1996.
32. Bonhoff, B., Tomm, U., and Johnson, B.V., "Heat Transfer Predictions for U-Shaped Coolant Channels with Skewed Ribs and with Smooth Walls," *ASME Paper* 96-TA-7, 1996.
33. Bonhoff, B., Tomm, U., Johnson, B.V., and Jennions, I., "Heat Transfer Predictions for Rotating U-Shaped Coolant Channels with Skewed Ribs and with Smooth Walls," *ASME Paper* 97-GT-162, 1997.
34. Stephens, M.A. and Shih, T.I-P., "Computation of Compressible Flow and Heat Transfer in a Rotating Duct with Inclined Ribs and a 180-Degree Bend," *ASME Paper* 97-GT-192, 1997.
35. Lin, Y.-L., Shih, T. I-P., Civinskas, K.C., Rigby, D.L., and Ameri, A.A., Nonlinear Versus Linear k-ω Model for Predicting Flow and Heat Transfer in a Smooth U-Duct, AIAA Paper 98-3560, July 1998.
36. Shih, T.I-P., Lin, Y.-L., Stephens, M.A., Chyu, M.K., and Civinskas, K.C., "Flow and Heat Transfer in a Ribbed U-Duct under Typical Engine Conditions," *ASME Paper* 98-GT-213, 1998.
37. Shih, T.I-P., Lin, Y.-L., Stephens, M.A., Chyu, M.K., and Civinskas, K.C., "Computation of Flow and Heat Transfer in a Smooth and a Ribbed U-Duct with and without Rotation," *ASME Paper* AJTE99/6266, ASME/JSME Joint Thermal Engineering Conference, March 1999.
38. Jang, Y.J., Chen, H.C., and Han, J.C., "Flow and Heat Transfer in a Rotating Square Duct with 45^o Angled Ribs by a Reynolds Stress Turbulence Model," ASME Paper 2000-GT-0229.
39. Lin, Y.-L., Shih, T.I-P., Stephens, M.A., and Chyu, M.K., "A Numerical Study of Flow and Heat Transfer in a Smooth and a Ribbed U-Duct with and without

Rotation," *ASME Journal of Heat Transfer*, Vol. 123, April 2001, pp. 219-232.
40. Shih, T.I-P., Lin, Y.-L., and Stephens, M.A., "Flow and Heat Transfer in an Internal Coolant Passage," *International Journal for Rotating Machinery*, Vol. 7, No. 5, September 2001, pp351-364.
41. Zehnder, F., Schüler, M., Weigand, B., von Wolfersdorf, J., and Neumann, S.O., "The Effect of Turning Vanes on Pressure Loss and Heat Transfer of a Ribbed Rectanguklar Two-Pass Internal Cooling Channel," ASME Paper GT2009-59482, 2009.
42. Schüler, M., Dreher, H.-M., Neumann, S.O., Weigand, B., and Elfert, M., "Numerical Predictions of the Effects of Rotation on Fluid Flow and Heat Transfer in an Engine-Similar Two-Pass Internal Cooling Channel with Smooth and Ribbed Walls," ASME Paper GT2010-22870, 2010.
43. Menter, F.R., Zonal Two-Equation k-ω Turbulence Models for Aerodynamc Flows, *AIAA Paper* 93-2906, 1993.
44. Menter, F.R. and Rumsey, C.L., Assessment of Two-Equation Turbulence Models for Transonic Flows, *AIAA Paper* 94-2343, 1994.
45. Wilcox, D.C., *Turbulence Modeling for CFD*, DCW Industries, Inc., La Canada, California, 1993.
46. Taslim, M.E., "Experimental Heat Transfer in Stationary Rib-Roughened Rectangular Channels," *Heat Transfer in Gas Turbines*, Editors: B. Sundén and M. Faghri, WIT Press, Ashurst, Southhampton, 2001, Chapter 8, pp. 291-405.
47. Taslim, M.E., "Experimental Heat Transfer in Roughened Leading- and Trailing-Edge and in Spanwise Rotating Ducts" *Heat Transfer in Gas Turbines*, Editors: B. Sundén and M. Faghri, WIT Press, Ashurst, Southhampton, 2001, Chapter 9, pp. 407-520.
48. Metzger, D.E., Shephard, W.B., Haley, S.W., "Row Resolved Heat Transfer Variations in Pin-Fin Arrays Including Effects of Non-Uniform Arrays and Flow Convergence," ASME Paper 86-GT-132, IGTI Conference and Exhibit, Dusseldorf, West Germany, 1986.
49. VanFossen, G.J., "Heat Transfer Coefficients for Staggered Arrays of Short Pin Fins," ASME J. of Engineering for Gas Turbine and Power, Vol. 104, No. 2, 1982, pp. 268-274.
50. Brigham, B.A. and VanFossen, G.J., "Length-to-Diameter Ratio and Row Number Effects in Short Pin Fin Heat Transfer," ASME J. of Engineering for Gas Turbine and Power, Vol. 106, 1984, pp. 241-245.
51. Lau, S.C., Kim, Y.S., and Han, J.C., "Effects of Fin Configurations and Entrance Length on Local Endwall Heat/Mass Transfer in a Pin Fin Channel," ASME Paper 85-WA/HT-62, 1985.
52. Chyu, M.K., "Heat Transfer and Pressure Drop for Short Pin-Fin Arrays with Pin-Endwall Fillet," ASME J. of Heat Transfer, Vol. 112, Nov., 1990, pp. 926-32.
53. Chyu, M.K., Natarajan, V., and Metzger, D.E., "Heat/Mass Transfer from Pin-Fin Arrays with Perpendicular Flow Entry," ASME HTD, Vol. 226, Fundamentals and Applied Heat Transfer Research for Gas Turbine Engines, 1992.
54. Chyu, M.K., Hsing, Y.C., Shih, T.I-P., and Natarajan, V., "Heat Transfer Contributions of Pins and Endwall in Pin-Fin Arrays: Effects of Thermal Boundary Condition Modelling," ASME Paper 98-GT-175, IGTI Conference and Exhibit, Stockholm, 1998.
55. Chyu, M.K., Yen, C.H., Ma, W., and Shih, T.I-P.," Effects of Flow Gap Atop Pin Element on the Heat Transfer from Pin Fin Arrays," ASME Paper 99-GT-047, June 1999.
56. Chyu, M.K., Hsing, Y., and Shih, T.I-P., "Heat Transfer Contributions of Pins and Endwall in Pin-Fin Arrays: Effects of Thermal Boundary Condition Modeling," *ASME Journal of Turbomachinery*, Vol. 121, No. 2, April 1999, pp. 257-263.
57. Shih, T.-H., Liou, W., Shabbir, A., and Zhu, J., "A New k-ε Eddy-Viscosity Model for High Reynolds Number Turbulent Flows – Model Development and Validation," *Computers and Fluids*, Vol. 24, No. 3, 1995, pp. 227-238.
58. Launder, B.E. and Spalding, D.B., "The Numerical Computation of Turbulent Flows," *Computer Methods in Applied Mechanics and Engineering*, Vol. 3, 1974, pp. 269-289.
59. Chen, H.C. and Patel, V.C., "Near-Wall Turbu-lence Models for Complex Flows including Separation," *AIAA Journal*, Vol. 26, No. 6, 1988, pp. 641-648.
60. Wolfshtein, M., "The Velocity and Temperature Distribution in One-Dimensional Flow with Turbulence Augmentation and Pressure Gradient," *International Journal of Heat and Mass Transfer*, Vol. 12, 1969, pp. 301-318.
61. http://www.fluent.com/software/fluent/index.htm.

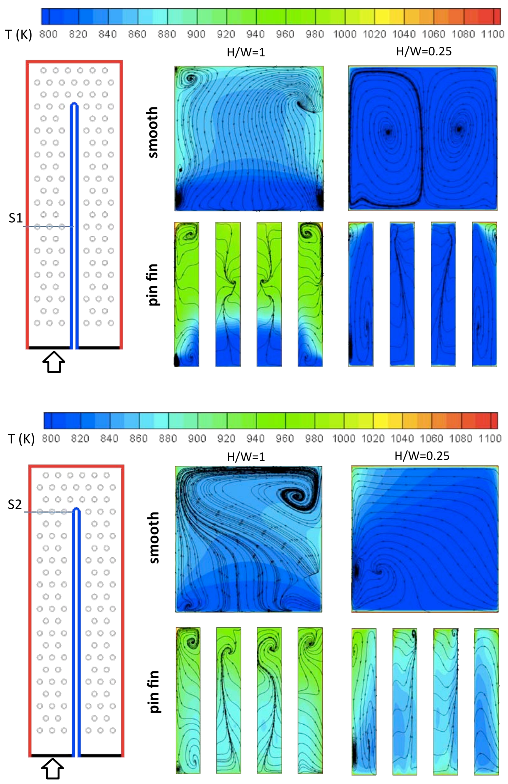

Fig. 6. Temperature (K) and projected streamlines at cross-sections S1 and S2 (Ω = 3,600).

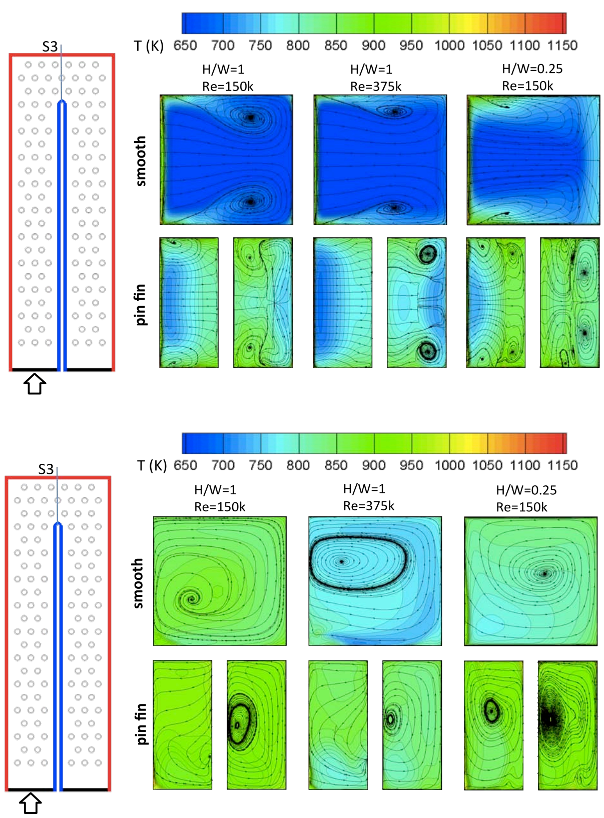

Fig. 7. Temperature (K) and projected streamlines at cross-section S3. Top: Ω = 0. Bottom: Ω = 3,600 rpm.

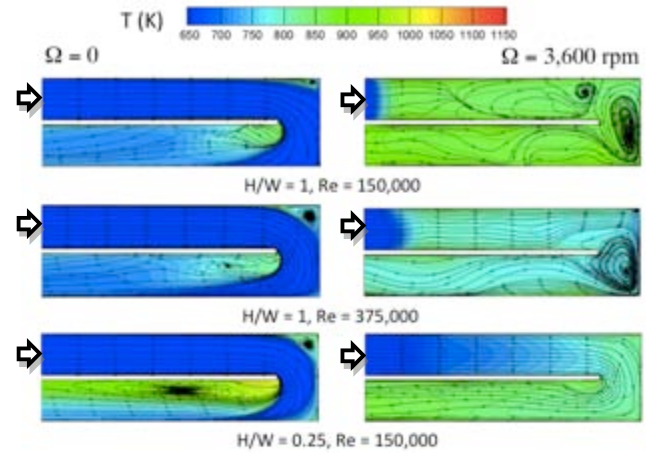

Fig. 8. Temperature and projected streamlines in the middle plane(Z=0) of smooth U-duct.

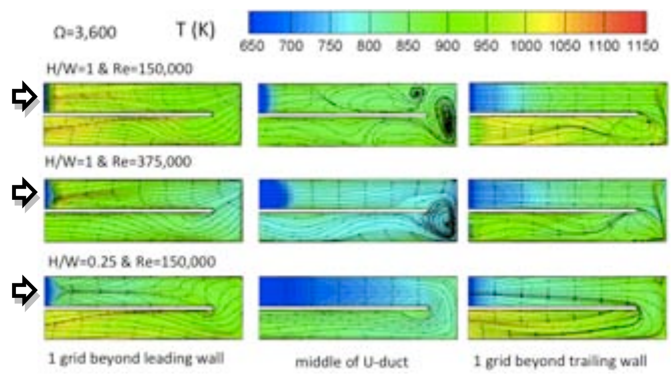

Fig. 9. Temperature and projected streamlines in several planes of smooth U-duct for Ω = 3,600 rpm.

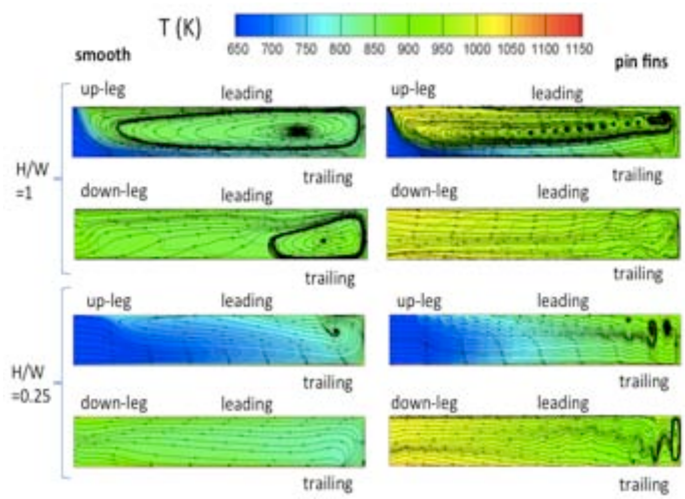

Fig. 10. Temperature (K) and projected streamlines at a cross-section at X = -(W-t/2)/2 in the up-leg duct and at X = (W-t/2) at the down-leg duct (Ω = 3,600 rpm).

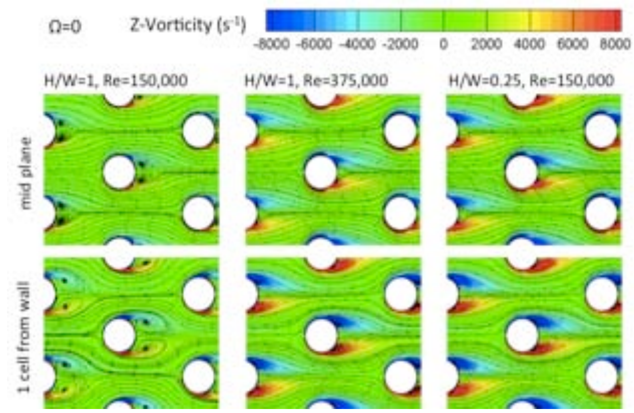

Fig. 11. Z-vorticity and projected streamlines on two planes in near the middle of the up-leg duct.

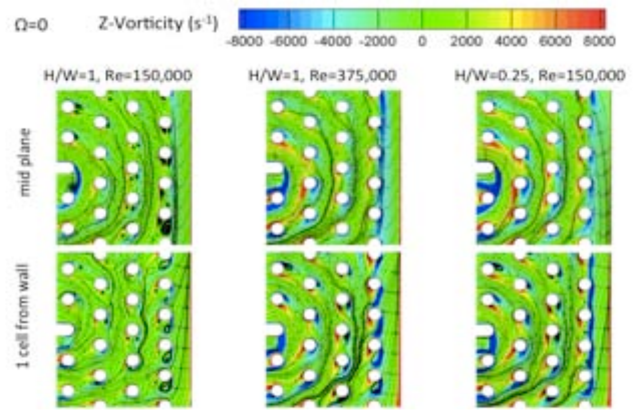

Fig. 12. Z-vorticity and projected streamlines on two planes in middle of the turn region.

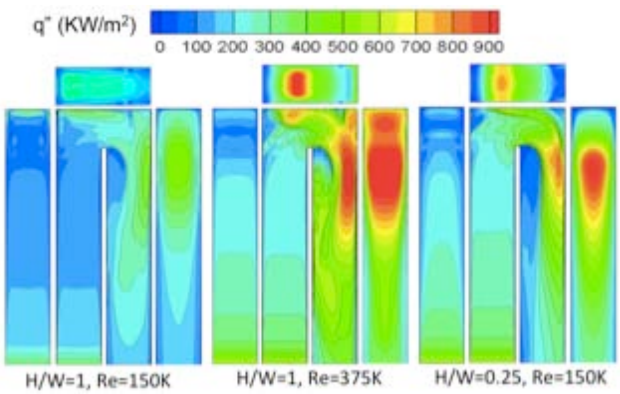

Fig. 13. Heat flux (W/m^2) on the walls of the smooth U-duct (Ω = 0). (Left duct is up-leg and right duct is down-leg)

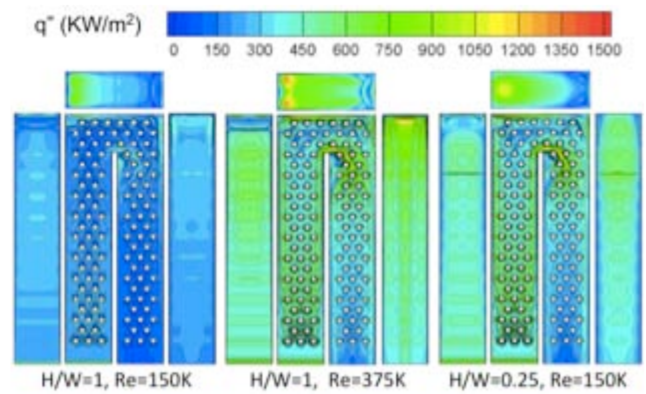

Fig. 14. Heat flux (W/m^2) on the walls of the pin-finned U-duct (Ω = 0). (Left duct is up-leg and right duct is down-leg)

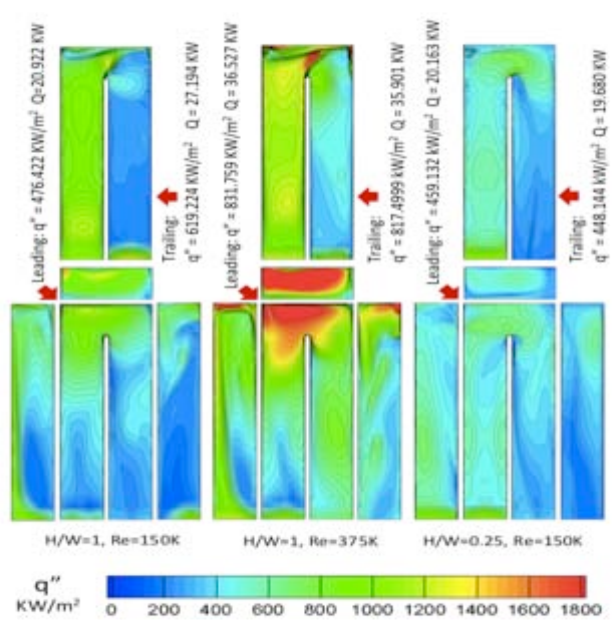

Fig. 15. Heat flux (W/m^2) on the walls of the smooth U-duct (Ω = 3,600 rpm). (Left duct is up-leg and right duct is down-leg)

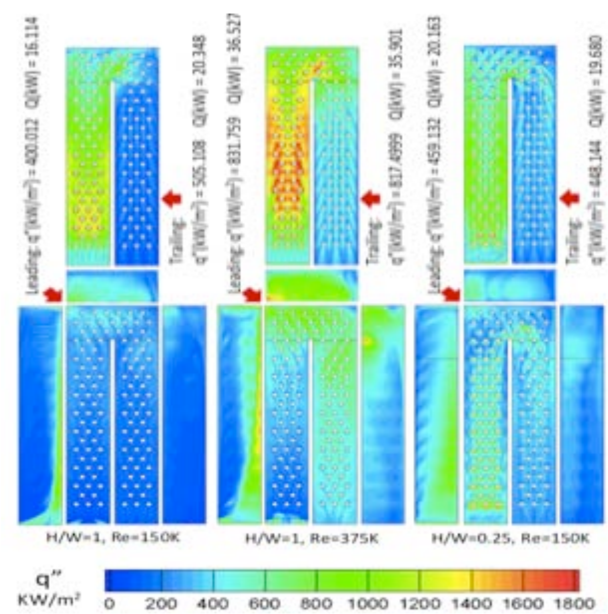

Fig.16. Heat flux (W/m^2) on the walls of the pin-finned U-duct (Ω = 3,600 rpm). (Left duct is up-leg and right duct is down-leg)

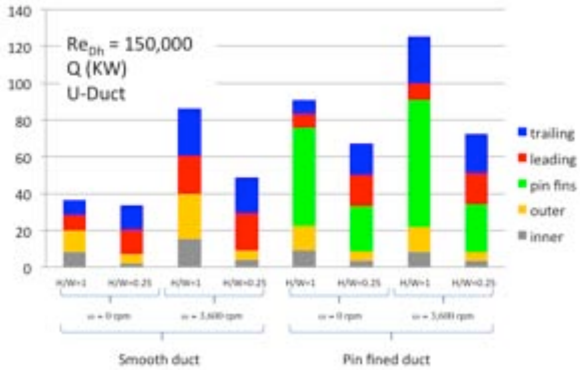

Fig. 17. Total heat transfer from U-duct.

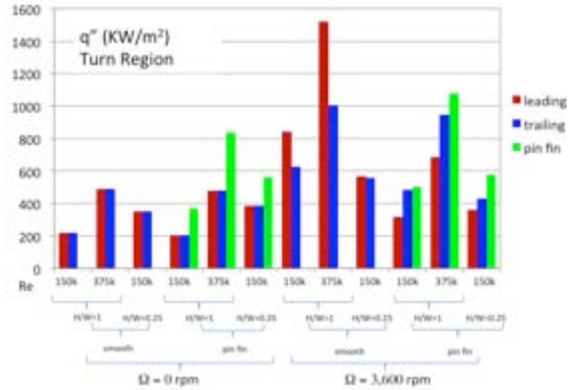

Fig. 21. Averaged heat flux from the turn region.

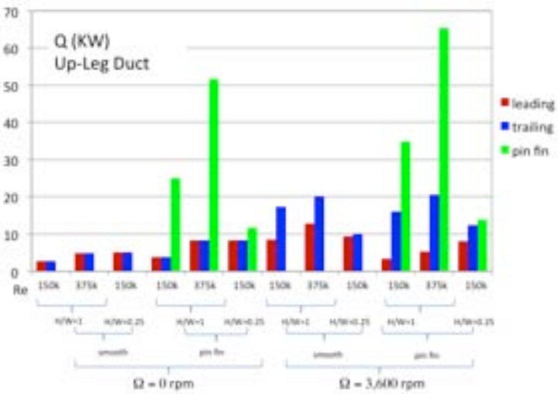

Fig. 18. Heat transfer from up-leg.

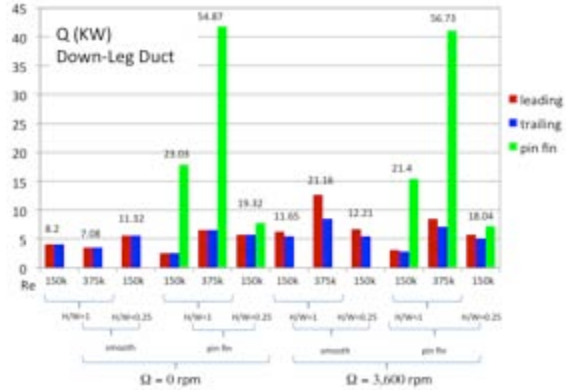

Fig. 22. Heat transfer from down-leg.

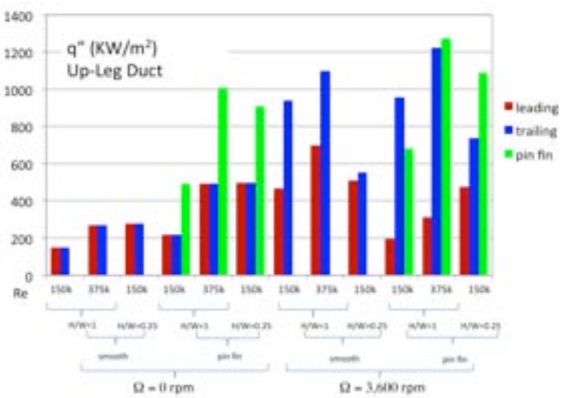

Fig. 19. Averaged heat flux from up-leg.

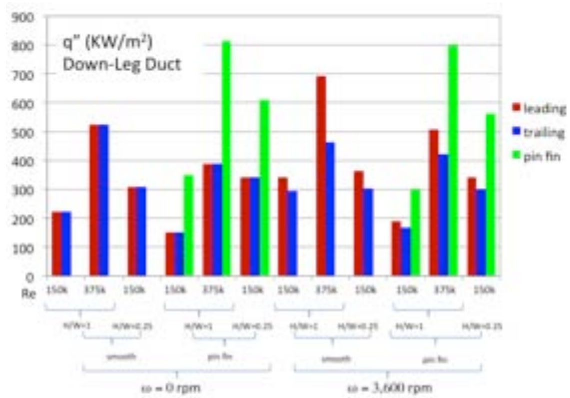

Fig. 23. Averaged heat flux from down-leg.

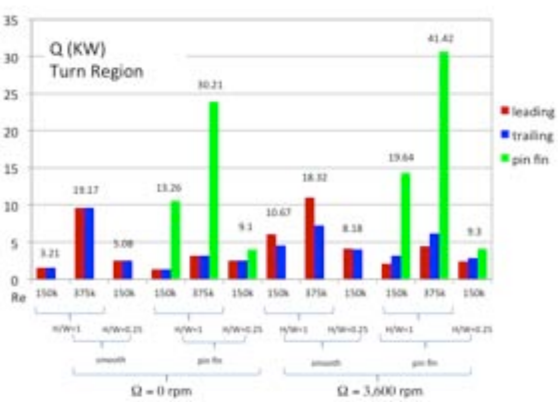

Fig. 20. Heat transfer from turn region.

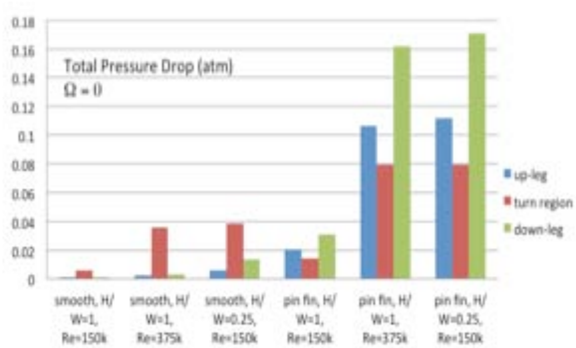

Fig. 24. Total pressure drop across U-duct (Ω = 0).

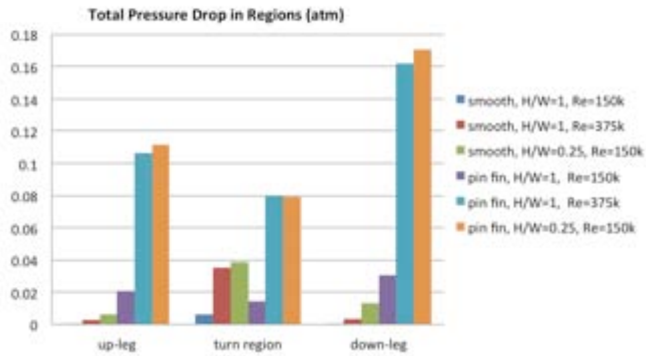

Fig. 25. Total pressure drop in up-leg, turn region and down-leg parts of the U-duct (Ω = 0).

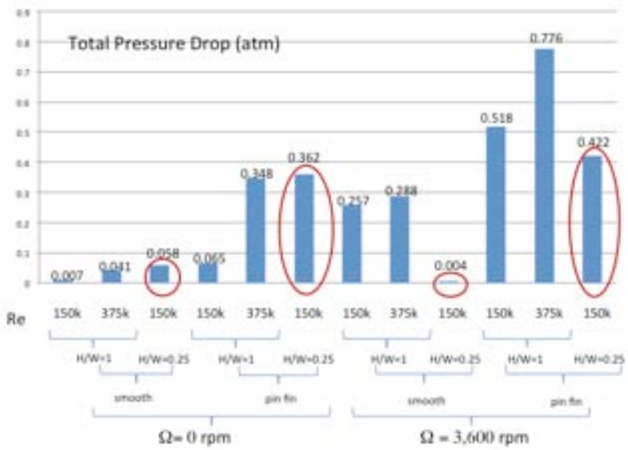

Fig. 26. Total pressure drop as a function of H/W, smooth versus pin-finned, and rotation.